ELSEVIER

The Science of the Total Environment 263 (2000) 209–219

the Science of the Total Environment
An International Journal for Scientific Research into the Environment and its Relationship with Man

www.elsevier.com/locate/scitotenv

Minerals controlling arsenic and lead solubility in an abandoned gold mine tailings

Christophe Roussel[a,*], Catherine Néel[a,b], Hubert Bril[a,b]

[a] *Laboratoire d'Analyse Structurale et Hydrothermalisme, Université de Limoges, 123 avenue Albert Thomas, 87060 Limoges cedex, France*

[b] *UMR 6532 CNRS, 123 avenue Albert Thomas, 87060 Limoges cedex, France*

Received 16 March 2000; accepted 8 July 2000

Abstract

Numerous areas have been contaminated by heavy metals and metalloids due to industrial and mining activities. Studies investigating the behavior of such contaminants in the environment have identified speciation as a key factor controlling their mobility, availability and toxicity. Here we characterize As- and Pb-bearing phases resulting from the oxidation of sulfide-rich tailings of a former gold mine (La Petite Faye, France) in order to assess the risk for water quality. Elements were first pre-concentrated by granulometric fractionation (sedimentation in deionized water) and then investigated using X-ray diffraction and electron microprobe analyses. Two main As–Pb-bearing minerals were clearly identified: scorodite ($FeAsO_4 \cdot 2H_2O$) and beudantite $PbFe_3(AsO_4)(SO_4)(OH)_6$. Minor amounts of As and Pb were dissolved in deionized water during granulometric fractionation, indicating the possible presence of other soluble Pb-sulfates which could be some of the primary metastable products of sulfide oxidation. This dissolution also provides information about the fate of these phases in the case of intensive leaching of the tailings. Scorodite may not be considered as a relevant candidate for As on-site immobilization, because its solubility largely exceeds drinking water standards whatever the pH. Since beudantite solubility has not yet been determined, an estimation of its solubility product was obtained using the Gibbs free energy of formation of plumbojarosite $[Pb_{0.5}Fe_3(SO_4)_2(OH)_6]$. This estimation suggests that beudantite should efficiently maintain low Pb concentration in waters. However, Pb dissolution in deionized water during the granulometric fractionation led to Pb concentrations much higher than the French and US drinking water standards (2.4×10^{-7} mol l^{-1}), which may be due to dissolution of the suspected metastable Pb-sulfates. Accurate determination of beudantite solubility is now required to improve the Pb risk assessment on such polluted sites.

Keywords: Arsenic; Lead; Scorodite; Beudantite; Solubility; Mine tailings

* Corresponding author. Tel.: +33-5-55-45-74-13; fax: +33-5-55-45-74-12.
E-mail address: roussel@unilim.fr (C. Roussel).

0048-9697/00/$ - see front matter
PII: S0048-9697(00)00707-5

1. Introduction

Historic mining and industrial activities have produced numerous sites containing high concentration levels of As, Pb, Zn and Cu in several regions of France. At La Petite Faye (Creuse dept., France), 34 000 t of gold ores were processed in the early 1960s and related wastes were left over the site. This material contained a variety of sulfides containing large amounts of arsenopyrite (FeAsS) and galena (PbS). Sulfides have been submitted to oxidation reactions since they were dumped under surface conditions. Such processes generate acidic conditions (Singer and Stumm, 1970), and induce contaminant releases (i.e. Pb, As, Zn, Cu, etc.) for which the fate and transport were investigated in a wide range of situations (e.g. Johnson and Thornton, 1987; Mok et al., 1988; Walter et al., 1994; Tin and Wilanders, 1995; Roussel et al., 1998).

Arsenic may be present in two main redox states [As(III) and As(V)] in natural waters (Ferguson and Gavis, 1972); changes in solubility and mobility therefore occur as a function of the redox potential and pH conditions in the environment (Wilson and Hawkins, 1978; Tallman and Shaikh, 1980; Pierce and Moore, 1982; Roussel et al., 2000). Some authors have noted an association between As(V) and Fe oxyhydroxides by co-precipitation (Mok et al., 1988; Masscheleyn et al., 1991), as well as the formation of Ca and Mg arsenates (Pierrot, 1964; Voigt et al., 1996; Juillot et al., 1999). It was also found that the presence of organic matter significantly increases arsenate adsorption (Cornu et al., 1999).

Oxidation of galena (PbS) results in the precipitation of a wide variety of secondary minerals, in which cerussite ($PbCO_3$), hydrocerussite [$Pb_3(CO_3)_2(OH)_2$] and anglesite ($PbSO_4$) are the most commonly reported (e.g., Davis et al., 1992; Hudson-Edwards et al., 1996). Numerous Pb phosphates may also be formed (Davis et al., 1993; Kalbasi et al., 1995; Morin et al. 1999) and are the Pb mineral phases of lowest solubility. Adsorption of Pb onto Fe- and, to a greater extent, Mn-oxides was also emphasized by several authors (McKenzie, 1980; Rauret et al., 1988; Morin et al., 1999).

Speciation is thus identified as a key factor controlling mobility, availability, and toxicity of metals and metalloid contaminants. In the present study, we aimed to characterize the main As- and Pb-bearing phases and their stability on the site of La Petite Faye. We used direct determination of the phases (spectrometry, diffractometry), which generally implies a pre-concentration step because of the technical detection limits. Since it is known that the concentration of trace elements such as As and Pb often increases with decreasing particle size (e.g. Chunguo and Zihui, 1988), we performed a particle size separation by sedimentation in deionized water. Interaction with deionized water may be compared to interaction with rainwater or natural waters having low total dissolved species. Although such pre-treatment may involve some metal-phase dissolution, thus increasing interpretation difficulties, it also provides information about the metals' behavior when the material is submitted to high leaching. Special attention was therefore paid to the chemical evolution of the water used for particle size separation.

2. Materials and methods

2.1. Site description

La Petite Faye tailings are located 60 km NE of Limoges, in the southwest of France. It forms a flat zone of variable thickness (1–5 m), which covers a small catchment (1 ha) along the Peyroux River. In a previous study based on the vegetal cover and particle size distribution, the site was found to be divided into three main parts from the upper zone to the river (Dutreuil et al., 1998). The highest metal concentrations (1–2 wt.% Pb, 6–7 wt.% As) and most acidic conditions (pH 2.5–3.5) were measured for material sampled in the upper part of the site.

2.2. Sampling and bulk characterization

Two samples were collected at 20 (S20) and 50 cm (S50) in the water unsaturated zone of the upper part of the site. Sample S20 was taken in a

brown layer, whereas S50 was yellow. Material was air-dried at 25°C in order to preserve trace elements speciation (Bordas and Bourg, 1998). Organic matter content was determined according to the Walkey-Black procedure (Jackson et al., 1984), and pH was measured in water (2:5 solid/water) according to the French standard X31-103 (AFNOR, 1994) using a HI 1230B combined electrode (3M KCl) connected to a HI 9025C pH/mV meter. Grain size distribution was obtained by sieving and sedimentation. Total sulfur concentrations were measured on the bulk material using inductively coupled plasma-mass spectrometry (ICP-MS). The material was digested in acid (Al-Shukry et al., 1992), and As, Pb and Fe concentrations were measured by graphite furnace atomic absorption spectrometry (GFAAS) on a Varian SpectrAA-800 Zeeman.

2.3. Experimental design

Material (50 g) was shaken for 24 h in 1 l deionized MilliQ water (initial pH 5.3) without any chemical addition in order to keep experimental conditions as close as possible to natural conditions (no defloculating agent, ionic strength and pH not adjusted). Particles were then allowed to settle in the shaking bottles and fractions < 2 μm (clay) and < 20 μm (fine silt) were separated with a siphon system allowing the collection of unsettled particle size fractions. Solids were separated from the water by filtration on 0.1-μm filters. The low % of fine grains required repetition of the solids collection (seven times) in order to provide enough material for chemical and mineralogical investigations. Shaking bottles were filled with freshly produced deionized water after each solid sampling (i.e. every 24 h).

Two sub-samples of each solid fraction were digested in acid for GFAAS chemical analysis. The mineralogical composition was determined by X-ray diffraction (XRD) performed on a Siemens D5000 diffractometer. Samples were X-rayed using CuKα radiation with a step size of 0.04°2θ and a count time of 10 s per step. The chemical composition of the As- and Pb-bearing material was investigated using a scanning electron microscope (SEM) (Phillips XL-30) and electron microprobe analysis (EMPA) with a CAMEBAX microprobe equipped with four wavelength dispersive spectrometers (WDS) (15 kV, 10 nA, 20 s counting time).

Table 1
Analytical data for graphite furnace atomic adsorption spectrometry[a]

Element	Detection limit (μmol l^{-1})	Accuracy (%)	Precision (%)
Pb	0.005	3	5
As	0.1	4	7
Fe	0.05	7	10

[a] Calibration curves were obtained from Merck standards solutions 1000 ± 2 mg l^{-1}

Water was collected for chemical analysis (two sub-samples) at each step. The pH was measured and samples for cations analyses were acidified (10 μl ml^{-1}) with Normapur concentrated nitric acid, and stored at 4°C until analyzed. Dissolved As, Pb and Fe concentrations were determined by GFAAS (analytical data in Table 1). Major elements concentrations were obtained by ionic chromatography (Dionex FX-100) on non-acidified sub-samples.

3. Results

3.1. Bulk characterization

The bulk material mineralogy was quartz, feldspar, illite, chlorite, biotite, muscovite, pyrite, arsenopyrite and galena. Organic matter content was 0.25% for the two samples and the pH values were as low as 2.5 (S20) and 3.0 (S50). Textural analysis showed that S50 and S20 contained 7 and 10.8% fine silt (2–20 μm), respectively. Both samples had a low clay fraction (3.3–3.6%). The total sulfur concentration was found to be lower in S20 (81 mmol kg^{-1}) than in S50 (106 mmol kg^{-1}).

3.2. Grain size fractionation of Pb and As

Bulk concentrations reached 2.9–5.8 wt.% Fe, 4–7.8 wt.% As and almost 1.5 wt.% Pb (Table 2). The clay fraction contained the highest As and Fe

Table 2
Average Pb, As and Fe concentrations (2 sub-samples) measured in bulk material and fine granulometric fractions

Sample	Pb (mg kg^{-1})	As (mg kg^{-1})	Fe (mg kg^{-1})
S50 (bulk)	14 600	41 150	29 660
2 < S50 < 20 μm	55 650	123 710	84 460
S50 < 2 μm	25 110	183 140	138 610
S20 (bulk)	14 910	78 150	58 230
2 < S20 < 20 μm	30 010	107 380	88 980
S20 < 2 μm	6 120	290 970	151 100

concentration, whereas Pb was mainly bound to the silt fraction. Arsenic and Fe were distributed following the order clay > silt > bulk, whereas Pb fractionation showed a decreasing concentration order following silt > clay > bulk (S50), or silt > bulk > clay (S20). Considering the fractions wt.% ([concentration in the fraction] × [fraction %]/[bulk concentration]), clay fractions contained 1.5–6% of the total Pb, 13.5–14.5% As, 9–15% Fe, and the fine silt fractions contained 21–27% Pb, 14–21% As, 16–20% Fe.

3.3. Characterization of As- and Pb-bearing minerals

Scanning electron microscopy showed that heavy elements are present in some omnipresent small flake-shaped aggregates (Fig. 1a) which contain Fe, As and Pb as shown on the EDS spectra (Fig. 1b). Minerals containing only Fe and As generally had a tabular appearance. The X-ray powder diffraction (Fig. 2) identified the presence of scorodite ($FeAsO_4 \cdot 2H_2O$) and beudantite [$PbFe_3(AsO_4)(SO_4)(OH)_6$]. Although none of the XRD patterns indicated other bearing mineral in these samples, this could be due to the detection limits and we could not confirm here that such minerals were not present in small quantities. A weak peak (9.96 Å) was also observed in sample S20, indicating that illite was present in this sample.

Plotting As, Fe and Pb concentrations from Table 2 in a ternary diagram (Fig. 3a) showed that most analyses are distributed on the As/Fe = 1:1 line, close to the Pb = 0 pole, indicating the predominance of 1:1 Fe arsenates. The EMPA data (Fig. 3b,c) also indicate that scorodite and beudantite are the major bearing minerals, but some of the plots seem to show that another Pb-phase was not identified in the XRD patterns. In the same way, location of the plots in Fig. 3a suggests that scorodite and beudantite were not the only mixing poles. In particular, plots for the < 2-μm fraction of sample S20 display an As enrichment, indicating the presence of a third As-bearing phase which was not detected by XRD analysis.

3.4. As and Pb release

Measurements of the solution pH after 24-h shaking with deionized water (removed and changed every 24 h, initial pH 5.3) exhibit an increasing pH trend for the two samples (Fig. 4). Very small amounts of metals were dissolved. Compared to the initial bulk concentrations, 0.04% As and 0.01% Fe were removed in solution. Dissolved As exhibited a minimum at pH 3.6–3.7 for the two samples (8×10^{-4} and 3×10^{-3} mmol l^{-1} for S50 and S20, respectively) and the final concentrations were approximately 2×10^{-3} mmol l^{-1} after seven shaking steps. Lead appeared to be much more soluble, with total dissolved % reaching 5% of the total sample content. Dissolved Pb concentrations decreased sharply from $6.0–7.8 \times 10^{-2}$ mmol l^{-1} to $7.5–4.5 \times 10^{-3}$ mmol l^{-1} (S20–S50) at the end of the experiment. Other dissolved species were mainly Na, K, NH_4, NO_3, Cl, and SO_4, which was by far the most concentrated. All the concentrations rapidly decreased with increasing leaching. A strong relationship was noted between dissolved SO_4 and Pb ($\log[SO_4] = 0.63 \pm 0.01 \log[Pb] - 1.00 \pm 0.04$; $R^2 = 0.95 \pm 0.02$), and a good negative correlation was also found when plotting Pb concentrations vs. pH (Fig. 4). However, it is clear that such correlations were not obtained from a standard solubility experiment and that we did not expect to provide a solubility product from the above relationship.

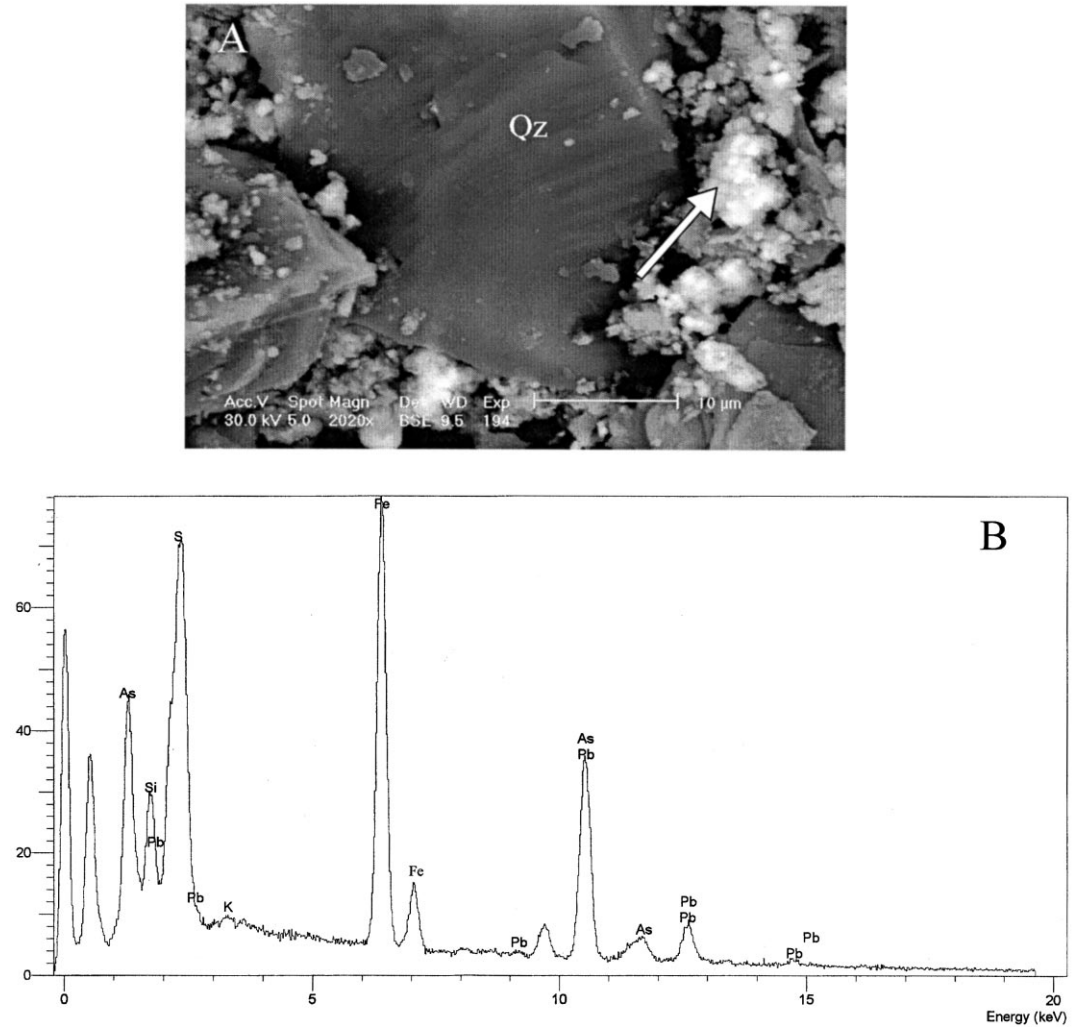

Fig. 1. a: SEM (backscattered electron) of the < 20-μm fraction (S50) showing quartz grain surrounded by high-contrast white flakes. b: EDS spectra indicating the As–Fe–Pb composition of the white flakes.

4. Discussion

4.1. As–Pb-bearing phases

Our results clearly show that sulfides were largely oxidized in the two studied samples, with the result that S molar concentrations are highly depleted compared to As and Pb. Two main As and Pb secondary phases were identified, which are consistent with a sulfide oxidation model. Arsenopyrite oxidation may result in dissolved arsenate and ferric iron release (Eq. (1)), or scorodite precipitation according to Eq. (2) as suggested by Dove and Rimstidt (1985). The combination of As, Fe and Pb released by oxidation of both arsenopyrite and galena (Eqs. (1) and (3)) results in the formation of beudantite (Eq. (4)).

$$FeAsS + \tfrac{7}{2}O_2 + H_2O \Rightarrow Fe^{3+} + SO_4^{2-} + H_2AsO_4^- \quad (1)$$

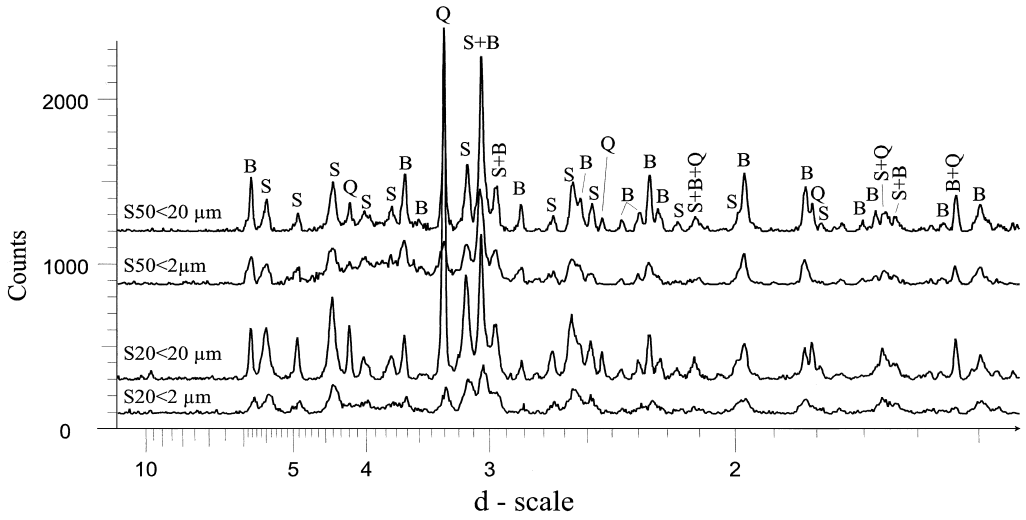

Fig. 2. XRD patterns of the < 2 μm and < 20 μm fractions (S50 and S20). Abbreviations: B, beudantite, S, scorodite, Q, quartz.

$$FeAsS + 14Fe^{3+} + 10H_2O \Rightarrow 14Fe^{2+} + FeAsO_4 \cdot 2H_2O + SO_4^{2-} + 16H^+ \quad (2)$$

$$PbS + H^+ \Rightarrow Pb^{2+} + HS^- \quad (3)$$

$$Pb^{2+} + 3Fe^{3+} + SO_4^{2-} + H_2AsO_4^- + 6H_2O \Rightarrow PbFe_3(AsO_4)(SO_4)(OH)_6 + 8H^+ \quad (4)$$

Although scorodite and beudantite were identified by direct determination, some of the As- and Pb-bearing phases were not seen using XRD, SEM observation or microprobe analyses. This is particularly clear for As in sub-samples S20 $<$ 2 μm (Fig. 3). Many Fe–As associations may occur in this kind of environment, ranging from As-rich Fe oxyhydroxides to well crystallized Fe arsenate such as those listed by Voigt et al. (1996). Most of these Fe arsenates have a Fe/As molar ratio higher than 1:1, except for kaatialaite [$Fe(H_2AsO_4)_3 \cdot 5H_2O$] for which Fe/As = 1:3. However, if it were present in sufficient quantities to explain the position of plots for S20 < 2 μm in Fig. 3, kaatialaite would have been clearly seen

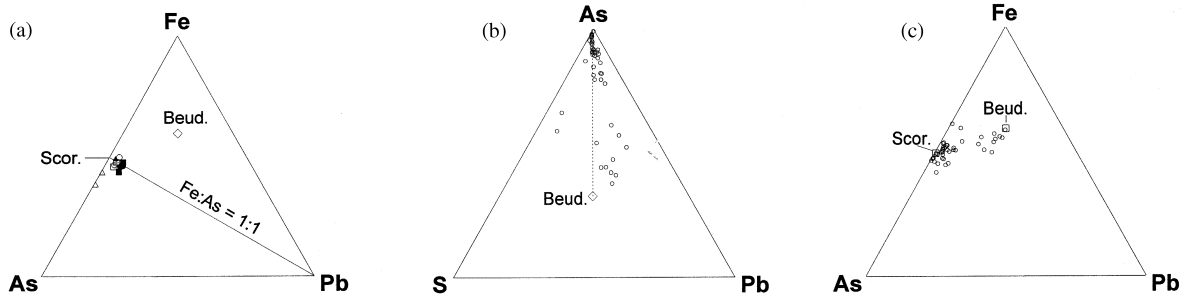

Fig. 3. a: Ternary diagram for As, Fe and Pb total concentrations measured in the bulk material, < 2-μm and < 20-μm fractions (duplicated analyses are plotted). Legend: squares, bulk material; circles, 2–20-μm fraction; triangle, < 2 μm. Symbols in black for sample S50 and in white for S20. b,c: Microprobe analyses of the As–Pb-bearing phases. Abbreviations: Scor., scorodite; Beud., beudantite.

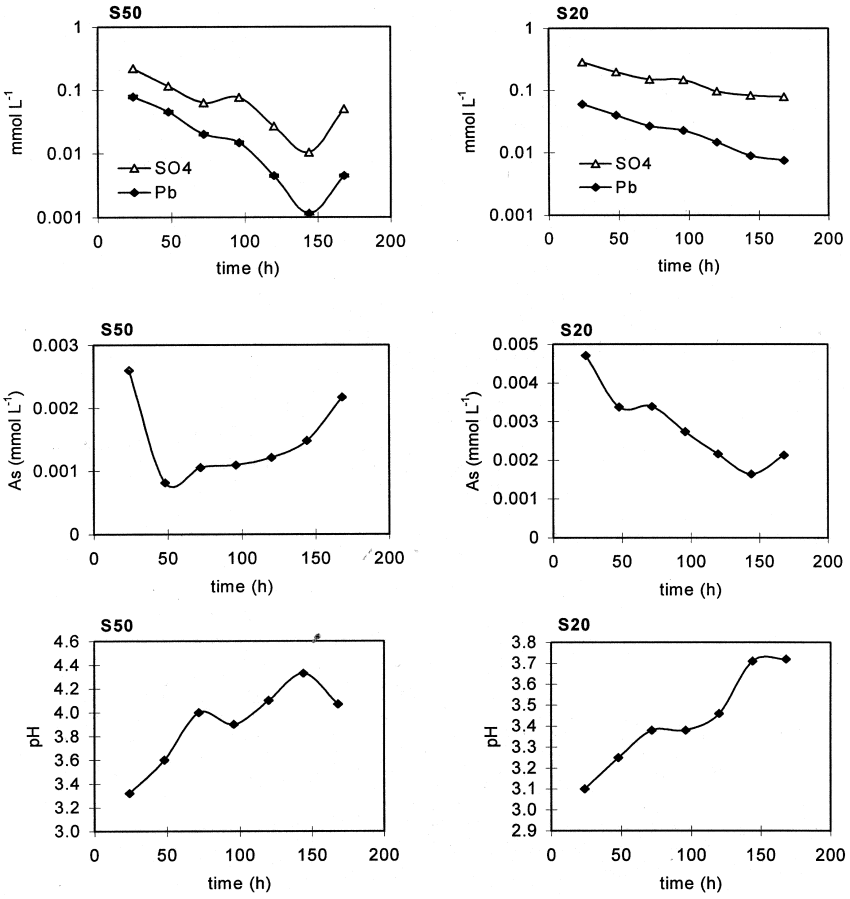

Fig. 4. Dissolved Pb, SO_4, As and pH measured vs. time. Water was removed and changed after each sampling.

on the XRD patterns (the main diffraction peaks at 9.91, 8.35 and 7.72 Å do not overlap with other mineral patterns). As a consequence, we do not believe that other Fe arsenates in addition to scorodite occur in this material. The organic matter (O.M.) content in our samples was also too low to consider that As ≡ O.M. complexes could explain the As enrichment seen in fraction < 2 μm (S20). As it is generally admitted that the < 2 μm fraction contains more clay minerals than others fractions, we suspect that As could be at least partially sorbed onto clay particles. This assumption is strongly supported by the fact that illite was effectively found in sample S20, and that illite edges possess positive charges, conferring to this mineral a strong ability to adsorb arsenic anions.

It was also found that beudantite is the main and not the only secondary Pb-bearing mineral. Indeed, Pb was the main dissolved metal found during size fractionation, and comparing As–Fe–Pb and S removal in some ternary diagrams (Fig. 5) strongly suggests another Pb-pole than beudantite. It also appeared in the As–Fe–Pb diagram that dissolved concentrations were not consistent with a mixing model between the identified minerals and the undetermined Pb-pole. If any dissolution of beudantite occurred, we can presume that Fe did not remain in solution and was rapidly precipitated as Fe oxyhydroxides, which could explain the fact that beudantite does not appear as a mixing pole in this diagram (Fig. 5a). Fig. 4 and the Fe–S–Pb diagram (Fig. 5b) suggest the dissolution of some

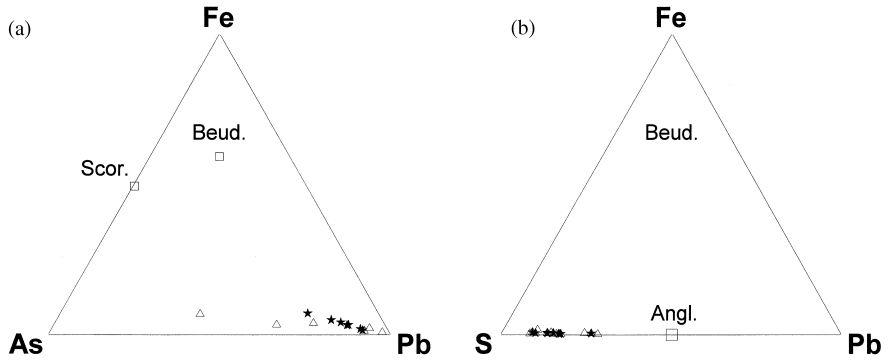

Fig. 5. a,b: Ternary diagrams for dissolved concentrations. Abbreviations: Scor., scorodite; Beud., beudantite; Angl., anglesite, $PbSO_4$. Black stars and white triangles for S20 and S50, respectively.

Pb-sulfates when the pH increases. These sulfates could be anglesite ($PbSO_4$) or many other more or less crystallized hydroxysulfates [e.g. $Pb(OH)(SO_4)_{0.5}$]. Nevertheless, these minerals constitute minor Pb-bearing phases compared to beudantite.

4.2. Stability of identified minerals

Scorodite is commonly found in association with As-bearing ore deposits as a weathering product and is known to be stable under oxidizing conditions in an acidic environment (Vink, 1996). Its solubility has been investigated and discussed by several authors (Dove and Rimstidt, 1985; Robins, 1987; Nordstrom and Parks, 1987; Krause and Ettel, 1988). Scorodite is metastable above pH 1.5 and its dissolution is congruent below pH 2.4, whereas it exhibits incongruency for higher pH values, resulting in iron hydroxide precipitation. The reported solubility products (Ksp) vary considerably from one author to another, from $Ksp = 10^{-21.7}$ (Dove and Rimstidt, 1985) to $Ksp = 10^{-24.4}$ (Krause and Ettel, 1988). Scorodite solubility was shown to be strongly dependent on pH with a minimum at $6.7\ 10^{-4}$ mmol l^{-1} at approximately pH 4.0 (i.e. equal to the As concentration limit for French and US drinking water standards), and sharply increases for lower and higher pH values (Krause and Ettel, 1988). Our results are quite consistent with these previous studies. The lowest As dissolved concentrations were obtained at pH 3.6–3.7 (Fig. 4) and dissolution increases above this value as shown for sample S50 (the trend of the curve suggests that it could also be expected for S20 if the experiment had been pursued further). The total dissolved As was very low compared to the total amount contained in the material, but As concentrations were higher than drinking standards whatever the pH. These results imply that scorodite is not a relevant candidate for As on-site immobilization because of the high As concentrations at equilibrium and the high pH-dependence for its stability.

Several studies have already investigated the structure of beudantite (e.g. Szymanski, 1988; Giuseppetti and Tadini, 1989), but parameters such as solubility are not available. Beudantite is structurally very close to the jarosite group for which the general formula is $AFe_3(SO_4)_2(OH)_6$ (where A may be K, Na, NH_4, H_3O, Ag, Pb, Ca, Sr or Ba). Anionic substitutions may occur in these minerals resulting in the replacement of some sulfate groups by $(AsO_4)^{3-}$ or $(PO_4)^{3-}$, and it has been shown that there is very little change in the unit-cell parameters upon replacement of a sulfate group by an arsenate in the jarosite structure (Jambor and Dutrizac, 1983). Some solid solutions have also been reported between K-jarosite, plumbojarosite [$Pb_{0.5}Fe_3(SO_4)_2(OH)_6$] and beudantite (Sànchez et al., 1996).

The solubility product (Ksp) of a given mineral is theoretically related to the Gibbs free energy of the dissolution reaction, following $Ksp = \exp(-\Delta G_r^\circ/RT)$. Because the beudantite Gibbs free energy of formation has also not yet been

determined, an approximation of its value was obtained using the Gibbs free energy of formation proposed by Kashkay et al. (1975) for Pb-jarosite (Table 3), assuming an equilibrium state between beudantite and Pb-jarosite, i.e. assuming that ΔG_f° (beudantite) could be expressed as in Eq. (5):

$$\Delta G_f^\circ(\text{beudantite}) = \Delta G_f^\circ(\text{Pb-jarosite}) - \Delta G_f^\circ(SO_4^{2-}) + 0.5\Delta G_f^\circ(Pb^{2+}) + \Delta G_f^\circ(H_2AsO_4^-) \quad (5)$$

This approach provides a relatively low solubility product of 10^{-15} ΔG_f° (beudantite) = -727.5 kcal mol^{-1}. The same type of estimation was performed using the ΔG_f° obtained by Baron and Palmer (1996) for K-jarosite, and provided a significantly different value for the beudantite solubility product (Ksp = 10^{-21}), which might make this estimation method questionable. However, we believe that the Ksp obtained from the Pb-jarosite data is the most reliable value because of the high structural and chemical similarity between beudantite and Pb-jarosite.

Assuming that beudantite dissolves congruently in the pH range 2–4.5, the stability diagram (Fig. 6) was developed using concentration data from Néel et al. (submitted). It is clear from this diagram that Pb concentrations should remain below the drinking water standard for Pb (2.4×10^{-7} mol l^{-1}) from pH 2.2 to 4.5 (Ksp = 10^{-15}) or for the full pH range (Ksp = 10^{-21}). However, Pb concentrations obtained when leaching solids with deionized water were very high, and remained 5–30 times greater than drinking water standards when leached concentrations were the lowest. We suspect that this Pb release is due to the presence of metastable Pb-sulfates that may be considered as the first oxidation products of galena. As an example, if Ksp = 10^{-15} for beudantite, anglesite (Ksp = $10^{-7.7}$) should be the Pb solubility limiting phase for pH < 2.0, corresponding to the high acidic conditions induced by sulfide oxidation. As acidity rapidly decreases after oxidation because of various natural buffering salts, such sulfates become unstable and may combine with Fe and arsenates to form beudantite.

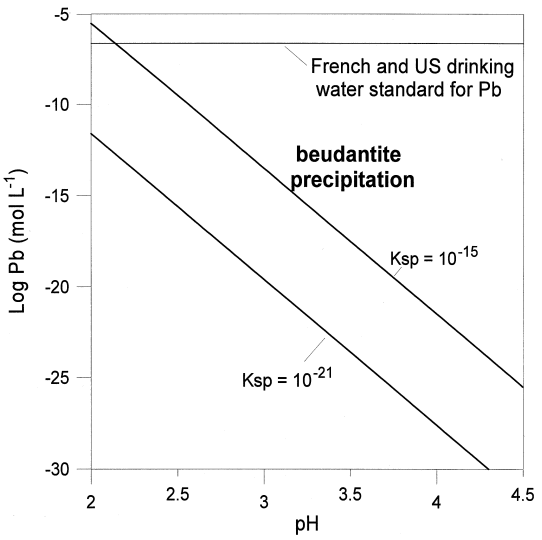

Fig. 6. Stability diagram for beudantite with Ksp = 10^{-15} and Ksp = 10^{-21}. Ionic activities were taken to be 1.8×10^{-6} mol l^{-1} for Fe^{3+}, 5.2×10^{-3} mol l^{-1} for SO_4^{2-} and 1.3×10^{-6} mol l^{-1} for $H_2AsO_4^-$.

Table 3
Selected thermodynamic data

Species	$\Delta G_{f,298}^\circ$ (kcal mol^{-1})	References
Pb-jarosite	−722.5	[a]
K-jarosite	−795.6	[b]
Pb^{2+}	−5.83	[c]
$H_2AsO_4^-$	−180	[c]
H_2O	−56.7	[c]
SO_4^{2-}	−177.9	[c]
K^+	−67.5	[c]

[a] Kashkay et al., 1975.
[b] Baron and Palmer, 1996.
[c] Wagman et al., 1982.

5. Conclusions

The particle size fractionation by sedimentation in deionized water was very efficient in preconcentrating the As- and Pb-bearing phases. The highest concentrations were measured in the fraction < 2 μm for As and in the fraction 2–20 μm for Pb. Although minor amounts of metals were

dissolved during the fractionation in water, these dissolutions provide information on behavior of the bearing phases when submitted to high leaching. For these special leaching conditions, in which the solid/solution ratio (1:20) is very low compared to the natural conditions occurring on the site, all the Pb and As concentrations were largely above the French and US drinking water standards of 6.7×10^{-7} and 2.4×10^{-7} mol l^{-1} for As and Pb, respectively.

Two main secondary minerals were found in these As–Pb-rich mine tailings. Arsenic is mainly in the form of scorodite ($FeAsO_4 \cdot 2H_2O$), and beudantite [$PbFe_3(SO_4)(AsO_4)(OH)_6$] is the main Pb-bearing mineral. The formation of sulfates such as anglesite ($PbSO_4$) as metastable primary products of galena oxidation is also strongly indicated by our results, although these minerals were not identified by direct determination (i.e. XRD, EMPA and SEM).

Scorodite and beudantite are the solubility-limiting phases of As and Pb, respectively. In accordance with previous studies on scorodite solubility, we found out that scorodite is not a relevant candidate for As in situ immobilization in polluted soil, due to the high pH dependence of its solubility and to high As concentrations at equilibrium. On the other hand, and despite a lack of knowledge concerning its solubility, our thermodynamic estimation reveals that the precipitation of beudantite should maintain low dissolved Pb concentrations. However, this conclusion has to be moderated because minor amounts of Pb are also included in much more soluble species (sulfates) resulting in potentially high Pb release in percolating water. An accurate determination of the beudantite solubility is also needed to improve the Pb risk assessment on this site.

References

AFNOR. Qualité des Sols. AFNOR, 1994.

Al-Shukry R, Serpaud B, Matejka G, Caullet C. Spéciation des métaux lourds d'un cours d'eau en aval d'un rejet industriel. Environ Technol 1992;13:129–140.

Baron D, Palmer CD. Solubility of jarosite at 4–35°C. Geochim Cosmochim Acta 1996;60:185–195.

Bordas F, Bourg ACM. A critical evaluation of sample pretreatment for storage of contaminated sediments to be investigated for the potential mobility of their heavy metal load. Water Air Soil Pollut 1998;103:137–147.

Chunguo C, Zihui L. Chemical speciation and distribution of arsenic in water, suspended solids and sediment of Xiangjiang river, China. Sci Total Environ 1988;77:69–82.

Cornu S, Saada A, Breeze D, Gauthier S, Barranger P. The influence of organic complexes on arsenic adsorption onto kaolinites. C R Acad Sci Earth Planet Sci 1999;328:649–654.

Davis A, Ruby MV, Bergstrom PD. Bioavailability of arsenic and lead in soils from the Butte, Montana, mining district. Environ Sci Technol 1992;26:461–468.

Davis A, Drexler JW, Ruby MV, Nicholson A. Micromineralogy of mine wastes in relation to lead bioavailability, Butte, Montana. Environ Sci Technol 1993;27:1415–1425.

Dove PM, Rimstidt JD. The solubility and stability of scorodite, $FeAsO_4 \cdot 2H_2O$. Am Mineral 1985;70:838–844.

Dutreuil JP, Bril H, Roussel C et al. Pédogénèse et réimplantation végétale sur les haldes d'une ancienne mine d'or (Massif Central français). International Soil Congress, Montpellier, 1998. 7p.

Ferguson JF, Gavis J. A review of the arsenic cycle in natural waters. Water Res 1972;6:1259–1274.

Giuseppetti G, Tadini C. Beudantite: $PbFe(SO_4)(AsO_4)(OH)_6$, its crystal structure, tetrahedral site disordering and scattered Pb distribution. Neue Jahnbuck für Mineralogie Monatshefte 1989;27-33.

Hudson-Edwards KA, Macklin MG, Curtis CD, Vaughan DJ. Processes of formation and distribution of Pb-, Zn-, Cd-, and Cu-bearing minerals in the Tyne basin, north-eastern England: implications for metal-contaminated river systems. Environ Sci Technol 1996;30:72–80.

Jackson JFC, Nevissi AE, Dervalle FB. Soil Chemical Analysis. Engelworks Cliffs, New Jersey: Prentice Hall Inc, 1984.

Jambor JL, Dutrizac JE. Beaverite–plumbojarosite solid solutions. Can Mineral 1983;21:101–113.

Johnson CA, Thornton I. Hydrological and chemical factors controlling the concentrations of Fe, Cu, Zn and As in a river system contaminated by acid mine drainage. Water Res 1987;213:359–365.

Juillot F, Ildefonse P, Morin G, Calas G, de Kersabiec AM, Benedetti M. Remobilization of arsenic from buried wastes at an industrial site: mineralogical and geochemical control. Appl Geochem 1999;14:1031–1048.

Kalbasi M, Peryea FJ, Lindsay WL, Drake SR. Measurement of divalent lead activity in lead arsenate contaminated soils. Soil Sci Soc Am J 1995;59:1274–1280.

Kashkay CM, Borovskaya YB, Babazade MA. Determination of G°_{f298} of synthetic jarosite and its sulfate analogues. Geochem Int 1975;5:115–121.

Krause E, Ettel V. Solubility and stability of scorodite, $FeAsO_4 \cdot 2H_2O$: new data and further discussion. Am Mineral 1988;73:850–854.

McKenzie RM, The adsorption of lead and other heavy metals on oxides of manganese and iron. Aust J Soil Sci 1980;18:61–73.

Masscheleyn PH, Delaune RD, Patrick Jr WH. Effects of redox potential and pH on arsenic speciation and solubility in a contaminated soil. Environ Sci Technol 1991;25: 1414–1419.

Mok WM, Riley JA, Wai CM. Arsenic speciation and quality of groundwater in a lead–zinc mine. Water Res 1988;22: 769–774.

Morin G, Ostergren JD, Juillot F, Ildefonse P, Calas G, Brown Jr GE. XAFS determination of the chemical form of lead in smelter-contaminated soils and mine tailings: importance of adsorption processes. Am Mineral 1999;84:420–434.

Néel C, Bril H, Courtin A, Dutreuil JP. Factors affecting natural development of soil on 35-year-old sulfide-rich mine tailings. Geoderma, submitted.

Nordstrom DK, Parks GA. Solubility and stability of scorodite, $FeAsO_4 \cdot 2H_2O$: discussion. Am Mineral 1987;72:849–851.

Pierce ML, Moore CB. Adsorption of arsenite and arsenate on amorphous iron hydroxide. Water Res 1982;16: 1247–1253.

Pierrot R. Contribution à la minéralogie des arséniates calciques et calcomagnésiens naturels. Bull Soc Fr Miner Crist 1964;87:169–211.

Rauret G, Rubio R, Lopez-Sanchez JF, Casassas E. Determination and speciation of copper and lead in sediments of a Mediterranean river (river Tenes, Catalonia, Spain). Water Res 1988;22:449–455.

Robins RG. Solubility and stability of scorodite, $FeAsO_4 \cdot 2H_2O$: discussion. Am Mineral 1987;72:842–844.

Roussel C, Bril H, Fernandez A. Hydrogeochemical survey and mobility of As and heavy metals on the site of a former gold mine (Saint-Yrieix mining district, France). Hydrogeology 1998;1:3–12.

Roussel C, Bril H, Fernandez A. Arsenic speciation: involvement in evaluation of environmental impact caused by mine wastes. J Environ Qual 2000;29:182–188.

Sànchez L, Cruells M, Roca A. Sulfidization-cyanidation of jarosite species: applicability to the gossan ores of Rio Tinto. Hydrometal 1996;42:35–49.

Singer PC, Stumm W. Acidic mine drainage: the rate determining step. Science N Y 1970;167:1121–1123.

Szymanski JT. The crystal structure of Beudantite, $Pb(Fe, Al)_3[(As, S)O_4]_2(OH)_6$. Can Mineral 1988;26:923–932.

Tallman DE, Shaikh AU. Redox stability of inorganic arsenic (III) and arsenic (V) in aqueous solution. Anal Chem 1980;52:196–199.

Tin NT, Wilanders A. Chemical conditions in acidic water in the Plain of Reeds, Vietnam. Water Res 1995; 29:1401–1408.

Vink BW. Stability relations of antimony and arsenic compounds in the light of revised and extended Eh–pH diagrams. Chem Geol 1996;130:21–30.

Voigt DE, Brantley SL, Hennet RJ-C. Chemical fixation of arsenic in contaminated soils. Appl Geochem 1996;11: 633–643.

Wagman DD, Evans WH, Parker VB et al. The NBS tables of chemical thermodynamic properties: selected values for inorganic and C1 and C2 organic substances in SI units of chemical thermodynamic properties. J Phys Chem Ref Data 1982;11(suppl. 2). 392 pp.

Walter AL, Frind EO, Blowes DW, Ptacek CJ, Molson JW. Modeling of multicomponent reactive transport in groundwater, 2. Metal mobility in aquifers impacted by acidic mine tailings discharge. Water Resour Res 1994;30: 3149–3158.

Wilson FH, Hawkins DB. Arsenic in streams, stream sediments, and ground water, Fairbanks area, Alaska. Environ Geol 1978;2:195–202.